Preprints of Control Conference Africa 2024
Balaclava, Mauritius, 16-17 September 2024

Model-Plant Mismatch Detection Using the Plant-Model Ratio: The Influence of Multivariable Systems Containing Both Fast and Slow Dynamics.

Heinz K. Mittermaier [*,**,1] **Johan D. le Roux** [**] **Ian K. Craig** [**]

[*] *Measurement and Control Division, Mintek, Randburg, South Africa.*
[**] *Department of Electrical, Electronic, and Computer Engineering, University of Pretoria, Pretoria, South Africa.*

Abstract: The plant-model ratio, developed to diagnose model-plant mismatch present in model-based controllers, inherits the same limitations from the frequency-based analysis that the method is based on. Nonetheless, the plant-model ratio shows the capacity to counteract the effect of non-linear dynamics within processes due to the ability to diagnose parametric model-plant mismatches for first-order plus time delay models. The plant-model ratio is developed before being validated on the Wood-Berry distillation column. One of the prominent limitations of frequency analysis, the filtering effects of time constant differences, is investigated and quantified for the Wood-Berry distillation column, showing the effect of time constant differences on each parametric model-plant mismatch diagnosis.

Keywords: controller performance monitoring, grinding mill circuit, model predictive control, model-plant mismatch, process performance monitoring.

1. INTRODUCTION

A key aspect influencing process control is the inevitability of changes in the process dynamics. These dynamic variations can lead to a decline in the performance of model-based controllers over time, consequently diminishing the advantageous outcomes associated with model predictive controllers (MPC). The challenge lies in addressing the impact of evolving dynamics to ensure the sustained effectiveness of control systems (Mayne, 2014; Qin and Badgwell, 2003; Schwenzer et al., 2021).

Both direct and indirect approaches to controller performance monitoring (CPM), specifically in the context of model-plant mismatch (MPM) detection and isolation have received significant attention to the point where discrepancies between the model and the plant can be identified seamlessly in real-time, with minimal disruptions to the ongoing process (Badwe et al., 2009; Jiang et al., 2009; Kaw et al., 2014; Li et al., 2020; Ling et al., 2017; Tsai et al., 2015; Wu and Du, 2022; Xu et al., 2020; Yin et al., 2014).

One of the promising methodologies of identifying, isolating and diagnosing MPM for multiple-input multiple-output (MIMO) systems consisting of first-order plus time delay (FOPTD) transfer functions is the plant-model ratio (PMR). The PMR was developed with the aim of identifying MPM followed by diagnosing the parameter mismatches present in a single-input single-output (SISO) FOPTD system (Selvanathan and Tangirala, 2010). The PMR was expanded to include MIMO system, which allowed the identification of MPM for the system, the isolation of the MPM to specific transfer functions within the transfer function matrix, and the diagnosis of parametric mismatches for each FOPTD model that contains MPM (Yerramilli and Tangirala, 2016). The method was initially tested on 2×2 systems (Yerramilli and Tangirala, 2018) as well as a 3×3 system in the form of a run-of-mine grinding mill circuit (Mittermaier et al., 2023) and showed promising results.

The PMR is fundamentally based on a frequency response analysis. Thus, the methodology will inherent basic frequency response requirements, for example, the requirement of broadband excitation as well as deviation variable models used in the PMR analysis (Mittermaier et al., 2023; Yerramilli and Tangirala, 2016).

A strong filtering effect can be seen in systems where a transfer function with a large time constant is present in the same row as one with a small time constant (Mittermaier, 2023). This filtering effect can be attributed to the fact that models with faster dynamics will have a shorter reaction time to inputs compared to the models with slower dynamics which will exclude the frequency-based information of the model with the slower dynamics when a frequency analysis of the system is conducted. Therefore, the difference in time constants is the foundation for the research and this article investigates the influence of time constant differences on diagnosing MPM using the PMR.

[1] Corresponding author, E-mail: HeinzM@mintek.co.za

2. PLANT-MODEL RATIO

The traditional form of MPM is defined as $\Delta G = G - \widehat{G}$, and can be derived from the internal model control (IMC) structure seen in Fig. 1. Due to modeling uncertainties and the lack of accurate process knowledge the traditional form of MPM (ΔG) is seldom zero. This led to the development of the PMR to diagnose MPM in model-based controllers using FOPTD plant representations. The PMR methodology allows not only for the identification of MPM but also the diagnosis of parametric mismatches in the form of a gain mismatch, a time constant mismatch, a time delay mismatch or a combination of these mismatches (Selvanathan and Tangirala, 2010).

2.1 PMR for SISO systems

The PMR for SISO systems is defined as the ratio between the process transfer function (G) and the model transfer function ($\widehat{G}$),

$$G_{PMR}(e^{j\omega}) = \frac{G(e^{j\omega})}{\hat{G}(e^{j\omega})} = M(\omega)e^{j\Delta P(\omega)}, \tag{1}$$

where $M(\omega)$ is the magnitude spectrum of the PMR and $\Delta P(\omega)$ is the phase spectrum of the PMR.

As discussed by Selvanathan and Tangirala (2010), the gain mismatch between the plant and the model is captured in the magnitude spectrum of the PMR ($M(\omega)$), while the delay mismatch is captured in the phase spectrum of the PMR ($P(\omega)$), the time constant mismatch is captured by both the magnitude and phase spectra of the PMR seen in (1).

As previously mentioned, the plant transfer function (G) will never be known at a 100% confidence level, thus the PMR will have to be estimated from routine closed-loop process data. The PMR estimation can be derived from the IMC structure of Fig. 1 by defining both the process and model outputs in terms of the manipulated variables and the output disturbances,

$$y(k) = Gu(k) + d(k) \tag{2}$$

$$\hat{y}(k) = \widehat{G}u(k). \tag{3}$$

In a noise-free environment, $v(k) = 0$, and the PMR estimation will be,

$$\frac{G(\omega)}{\widehat{G}(\omega)} = \frac{Y(\omega)}{\hat{Y}(\omega)}, \tag{4}$$

where $Y(\omega)$ and $\hat{Y}(\omega)$ are the Fourier transforms of y and $\hat{y}$ respectively. Nonetheless, for a practical system, the presence of noise and disturbances are unavoidable and a smoothed estimation of the PMR is desired. Building on an empirical transfer function estimation, the cross-spectral

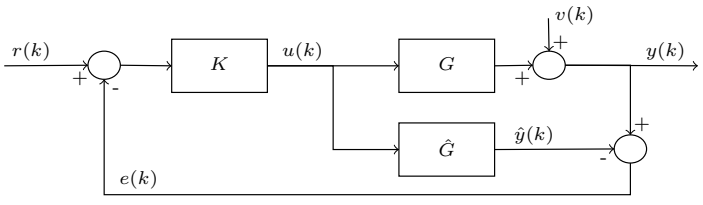

Fig. 1. Closed-loop IMC structure.

density (CSD) forms the foundation of the smoothed PMR estimation (Ljung, 1999; Selvanathan and Tangirala, 2010),

$$\widehat{G}_{PMR} = \frac{\gamma_{y,r}(\omega)}{\gamma_{\hat{y},r}(\omega)}, \tag{5}$$

where $\gamma_{y,r}(\omega)$ is the CSD between the process output y and the setpoint r, while $\gamma_{\hat{y},r}(\omega)$ is the estimated CSD between the model output $\widehat{y}$ and the setpoint r. The effect of noise and disturbances should be uncorrelated with the setpoint, and therefore the correlation analysis should remove both noise and disturbances from the PMR (Selvanathan and Tangirala, 2010; Yerramilli and Tangirala, 2016).

2.2 Improved PMR for SISO systems

As mentioned by Mittermaier et al. (2023), the PMR of Section 2 requires high-frequency setpoint excitation to ensure accurate MPM detection within the delay term of the FOPTD model. Thus, an improved PMR method is derived by using an optimal delay estimation technique to replace the reliance on the phase spectra of the PMR, and in turn, alleviate the requirement of high-frequency excitation applied to the setpoint as well as remove the low-pass filtering effect of the high-frequency excitation caused by the feedback control system. The optimal delay estimation technique stems from the fact that a discrete transfer function can be split into a delay-free term and a delay term,

$$G_{PMR}(z) = \underline{G_{PMR}}(z)z^{-\Delta D}, \tag{6}$$

where $\Delta D = D - \hat{D}$.

The phase spectrum of the transfer function contains a contribution from both the time-delay and delay-free part of the transfer function:

$$\arg[G_{PMR}(z)] = \arg[\underline{G_{PMR}}(z)] - \Delta D, \tag{7}$$

where arg represents the angle of the complex number. Therefore, if the left-hand side and the delay-free contribution of (7) is known, the delay (D) can be estimated. Using the fact that the magnitude spectrum of the delay-free term and the magnitude spectrum of the complete transfer function are equal, the angle of the delay-free term can be estimated using a discrete version of the Hilbert transform,

$$\begin{aligned}\arg\left[\underline{G_{PMR}}\left(\omega_l\right)\right] = \frac{1}{2B}\sum_{k=1,k\neq l}^{B}\log\left|G_{PMR}\left(\omega_k\right)\right| \times \\ \left(\cot\left(\frac{\omega_l-\omega_k}{2}\right)+\cot\left(\frac{\omega_l-\omega_k}{2}\right)\right),\end{aligned} \tag{8}$$

where ω_l is the frequency in question, while ω_k forms a moving window of frequencies within a bandwidth of frequencies denoted B (Lindemann et al., 2001). From (6) and (8) the delay mismatch can be estimated by solving the following cost function as proposed by Hamon and Hannan (1974),

$$\begin{aligned}\Delta\widehat{D} = \arg\max_{\Delta D}\sum_{B} W(\omega)\cos\left(\arg[G_{PMR}(\omega)]\right. \\ \left. - \arg[\underline{G_{PMR}}(\omega)] + \Delta D\omega\right),\end{aligned} \tag{9}$$

with a weighting function,

$$W(\omega) = \frac{\kappa^2(\omega)}{1-\kappa^2(\omega)}, \tag{10}$$

derived from a least-squares approach (Ljung, 1999), where $\kappa^2(\omega)$ is the magnitude-squared coherence between the input and output of the PMR (Mittermaier, 2023; Yerramilli and Tangirala, 2018).

2.3 The PMR expanded to MIMO systems

To expand the SISO PMR and develop a method of detecting MPM for MIMO systems, the plant output (y_i) of the IMC structure in Fig. 1 can be expressed in terms of the model output ($\widehat{y}_i$),

$$\begin{aligned} y_i(\omega) &= \sum_{k=1}^{n} G_{ik}(\omega)u_k(\omega) + d_i(\omega) \\ &= \sum_{k=1}^{n} G_{PMR_{ik}}(\omega)\hat{G}_{ik}(\omega)u_k(\omega) + d_i(\omega) \\ &= \sum_{k=1}^{n} G_{PMR_{ik}}(\omega)\hat{y}_{ik}(\omega) + d_i(\omega), \end{aligned} \tag{11}$$

where $\hat{y}_{ik}$ is the k-th component of the i-th model output, corresponding to the k-th input u_k. Thus, for an $n \times n$ MIMO system, the element-wise division between the plant and model transfer function matrices defines the PMR matrix (Mittermaier et al., 2023; Yerramilli and Tangirala, 2016, 2018),

$$\begin{aligned} G_{PMR}(\omega) &= \begin{bmatrix} \frac{G_{11}(\omega)}{\hat{G}_{11}(\omega)} & \frac{G_{12}(\omega)}{\hat{G}_{12}(\omega)} & \cdots & \frac{G_{1n}(\omega)}{\hat{G}_{1n}(\omega)} \\ \vdots & \vdots & \ddots & \vdots \\ \frac{G_{n1}(\omega)}{\hat{G}_{n1}(\omega)} & \frac{G_{n2}(\omega)}{\hat{G}_{n2}(\omega)} & \cdots & \frac{G_{nn}(\omega)}{\hat{G}_{nn}(\omega)} \end{bmatrix} \\ &= \begin{bmatrix} G_{PMR_{11}} & G_{PMR_{12}} & \cdots & G_{PMR_{1j}} \\ \vdots & \vdots & \ddots & \vdots \\ G_{PMR_{i1}} & G_{PMR_{i2}} & \cdots & G_{PMR_{ij}} \end{bmatrix}. \end{aligned} \tag{12}$$

Due to the coupling effect between all inputs and all outputs of a MIMO system, the systematic diagnosis of Table 1 cannot be trivially applied to the MIMO expansion of the PMR as seen in (12) (Mittermaier et al., 2023). To alleviate the coupling effect in MIMO systems, a partial cross-spectral density (PCSD) analysis (as described by Priestley (1981)) or a multiple linear regression method (as described by Yerramilli and Tangirala (2018)) can be used to estimate the PMR from routine operational data. This approach will result in a matrix of decoupled PMRs that can be treated analogously to (5) when applying the MPM diagnosis procedure as described in Table 1 to each entry in the PMR matrix.

The multiple linear regression method, also referred to as the implicit PMR estimation, stems from the idea that multiple linear regressions can be performed on (11) by first correlating both sides of (11) with the relevant setpoints, as shown in (13). This is required for the i-th row of G_{PMR} and will realize n unknown PMRs for each row. Once again the correlation with the setpoint should annul the effects of noise and disturbances since both these occurrences should be uncorrelated with the setpoints.

$$\begin{bmatrix} \gamma_{y_i,r_1}(\omega) \\ \vdots \\ \gamma_{y_i,r_n}(\omega) \end{bmatrix} = \begin{bmatrix} \gamma_{\hat{y}_{i1},r_1}(\omega) & \cdots & \gamma_{\hat{y}_{in},r_1}(\omega) \\ \vdots & \ddots & \vdots \\ \gamma_{\hat{y}_{i1},r_n}(\omega) & \cdots & \gamma_{\hat{y}_{in},r_n}(\omega) \end{bmatrix} \begin{bmatrix} G_{PMR_{i1}}(\omega) \\ \vdots \\ G_{PMR_{in}}(\omega) \end{bmatrix}. \tag{13}$$

From (13), i-th row of the PMR can be estimated via regression and (13) will have to be repeated for each row in the PMR matrix. The implicit method of estimating each entry in the PMR matrix equates to a matrix containing $n \times n$ entries that are homogeneous to the SISO PMR as shown in (5). The implicit method will be used in Section 3 because of the computational simplification compared to the explicit method.

Table 1. MPM diagnostic procedure using the improved PMR.

Step	**Assessment Procedure**	**Diagnosis of MPM**	**MPM Direction**
1	$M(\omega)\|_{\omega=0} \neq 1$	if $M(0) = 1$: $K = \hat{K}$, else $K \neq \hat{K}$	$M(\omega) > 1$ if $K > \hat{K}$, $M(\omega) < 1$ if $K < \hat{K}$
2	$M(\omega)$ has a zero slope (flatness test)	if flat: $\tau = \widehat{\tau}$, else $\tau \neq \widehat{\tau}$	$M(\omega)\|_{\omega=\pi} < 1$ if $\tau > \hat{\tau}$, $M(\omega)\|_{\omega=\pi} > 1$ if $\tau < \hat{\tau}$
3	Optimal delay mismatch detection		

The limitations of the PMR, as discussed by Selvanathan and Tangirala (2010) and Yerramilli and Tangirala (2016, 2018), are,

- **Set-point excitation -** Since the PMR is fundamentally based on frequency analysis, broadband excitation is required at the set-point to ensure that adequate information is obtained over more than a single frequency when conducting the PMR.
- **Deviation variable model -** To ensure that a large DC element does not overpower the PMR, deviation variable models should be used. Centering all models of the system about zero would ensure that the frequency spectrum analysis is coherent over the entire band of interest.

Mittermaier (2023) then expands on these limitations, especially when considering the MIMO implementation of the PMR,

- **Gain scaling -** Since the estimation of the MIMO PMR matrix includes a ratio between all process outputs and model outputs as seen in (13), it is evident, from the mathematical formulation of the CSD (Oppenheim, 1999), that the absolute size of the signals will influence the absolute size of the CSD and therefore the PMR might be overpowered by transfer functions not having gains within the same order. This effect can be mitigated by normalizing the gains of all models (Skogestad and Postlethwaite, 2010).
- **Time constant differences -** From the polar representation of the PMR used to develop the systematic diagnosing procedure of Table 1, it is evident that both the magnitude spectrum as well as the phase spectrum are influenced by a time constant mismatch (Yerramilli and Tangirala, 2018). Therefore, if there are time constant differences within the transfer function matrix being diagnosed (i.e., there are transfer functions with very fast dynamics and transfer functions with very slow dynamics relative to one another), a filtering effect will take place resulting in the loss of frequency-based information required for the PMR.

3. SIMULATION STUDY

To determine the effects that time constant differences have on the PMR, a simulation study was conducted. This includes a baseline simulation to ensure the effectiveness of the PMR in detecting MPM, followed by multiple simulations where the dynamics of the system were altered to investigate the relative consequences of the time constant differences.

3.1 Process Description

The Wood-Berry distillation column model, which is a 2×2 model consisting of FOPTD transfer functions, is used to quantify the effect of time constant differences (Wood and Berry, 1973).

$$\begin{bmatrix} y_1(s) \\ y_2(s) \end{bmatrix} = \begin{bmatrix} \frac{12.8e^{-s}}{16.7s+1} & \frac{-18.9e^{-3s}}{21s+1} \\ \frac{6.6e^{-7s}}{10.9s+1} & \frac{-19.4e^{-3s}}{14.4s+1} \end{bmatrix} \begin{bmatrix} u_1(s) \\ u_2(s) \end{bmatrix} \tag{14}$$

u_1 is the reflux flow rate, u_2 is the steam flow rate, y_1 is the overhead product composition and y_2 is the bottom product composition.

As mentioned by Yerramilli and Tangirala (2016), MPM for the gain and time constant terms can be introduced into the plant using the parameters in (15).

$$\Delta K_{ij} : \begin{bmatrix} 10\% & 15\% \\ -15\% & -10\% \end{bmatrix} \tag{15a}$$

$$\Delta \tau_{ij} : \begin{bmatrix} 10\% & 12\% \\ -15\% & -8\% \end{bmatrix} \tag{15b} \quad \Delta D_{ij} : \begin{bmatrix} 0\,T_s & T_s \\ 2\,T_s & 0\,T_s \end{bmatrix}, \tag{15c}$$

where T_s is the sampling time.

3.2 Simulation Description

The plant of (14) is controlled using a linear constrained MPC, with a pseudo-random binary reference trajectory to ensure adequate broadband excitation is applied to the system. Additive white Gaussian noise signals are added to each output to simulate measurement noise. The MPM mentioned in Section 3.1 will be applied to all simulations. For the simulations containing time constant differences in Section 3.4 and Section 3.5, both the plant and the controller models will be updated based on the dynamics being tested, but the MPM will only be applied to the plant models and not the controller models.

3.3 Baseline Simulation

To verify the PMR of Section 2 on the Wood-Berry distillation column, a baseline simulation is used. From the zero-frequency component of the PMR magnitude spectrum, it is evident that the PMR can detect, and diagnose the direction and the relative size of the gain MPM for all transfer functions as compared to (15a),

$$\Delta K = \left(\begin{bmatrix} 1.10 & 1.14 \\ 0.82 & 0.89 \end{bmatrix} - 1 \right) \times 100 = \begin{bmatrix} 10.0\% & 14.4\% \\ -18.0\% & -11.3\% \end{bmatrix} \tag{16}$$

To detect the time constant MPM, a linear line is fitted to the initial slope of the PMR magnitude spectra. The frequency range of [0 0.4] is used as recommended by Yerramilli and Tangirala (2018). The relative time constant mismatches can then be calculated by multiplying the gradient of the linear line with -100 to obtain a relative mismatch term, as seen in (17). It should be noted, as mentioned by Selvanathan and Tangirala (2010), that the time constant mismatch is only able to diagnose the direction of the mismatch and the relative sizes of the mismatch as compared to other time constant mismatches.

$$\Delta \tau = \begin{bmatrix} -0.21 & -0.23 \\ 0.37 & 0.23 \end{bmatrix} \times -100 = \begin{bmatrix} 20.85 & 23.09 \\ -37.49 & -23.40 \end{bmatrix} \tag{17}$$

To diagnose the time delay mismatch present in the system, the objective function of (9) was solved. The solutions of the objective function diagnosed a 2 sample delay in transfer function G_{21}, which corresponds to the applied MPM in (15c).

3.4 Simulation containing time constant differences for G_{11}

The transfer function G_{11} in (14) is altered as follows,

$$\frac{12.8e^{-s}}{(16.7 \times \nu)s + 1}, \tag{18}$$

where ν is a linear sweep multiplication factor with the range [1 10]. In other words, the time constant τ_{11} is swept up to a factor of 10. For each instance of the sweep, all of the parameter mismatches applied as in (15) will be evaluated. The results are graphed to compare the impacts of the variation in τ_{11}. If the time constant differences do not affect the PMR, the parametric mismatch graphs should correspond to the case where $\nu = 1$, i.e., remain constant over the entire range of ν.

As summarized in Table 2, the simulations conducted for each instance of ν are: no MPM, only gain MPM, only time constant MPM, only time-delay MPM, and MPM for all parameters. The gain, time constant and delay mismatches for the time constant sweep of G_{11} can be seen in Figs. 2 to 4.

3.5 Simulation containing time constant differences for G_{21}

The same time constant sweep of Section 3.4 is performed by altering the transfer function G_{21} in (14) as follows,

$$\frac{6.6e^{-7s}}{(10.9 \times \nu)s + 1}, \tag{19}$$

where ν is a linear sweep multiplication factor with the range [1 10].

The simulations summarized in Table 2 are also conducted for all time constant sweeps of G_{21}. The gain, time constant and delay mismatches for the time constant

Table 2. Time constant difference simulation legend.

Simulation	Description	Line color
1	No MPM present	
2	Only gain MPM present	
3	Only time constant MPM present	
4	Only time delay MPM present	
5	Full MPM present	

sweeps of G_{21} can be seen in Figs. 5 to 7. It should be noted, due to the formulation of the time constant mismatch diagnosis $\left(\left|\frac{G_{PMR(0)}}{G_{PMR}(\omega)}\right|\right)$ that the numerator of the PMR could equate to zero, realizing an undefined value for the time constant mismatch. This can be seen for larger ν values in Fig. 6.

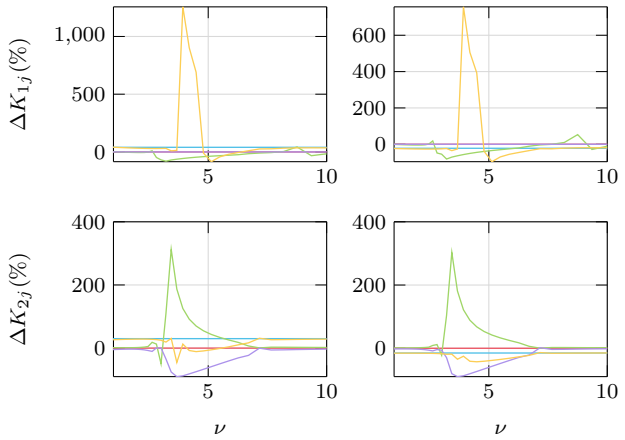

Fig. 2. Gain mismatches for time constant difference simulation of G_{11}.

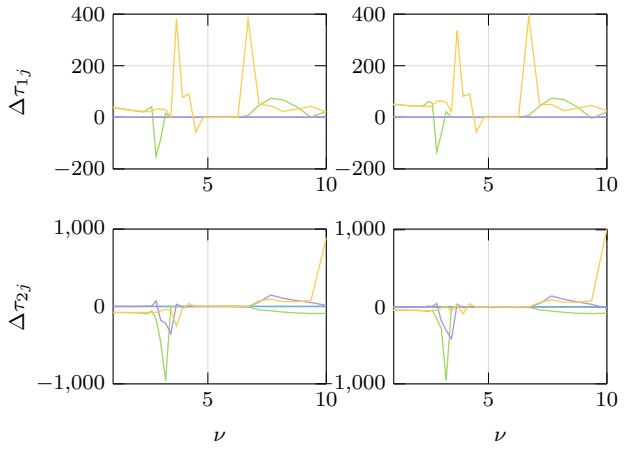

Fig. 3. Time constant mismatches for time constant difference simulation of G_{11}.

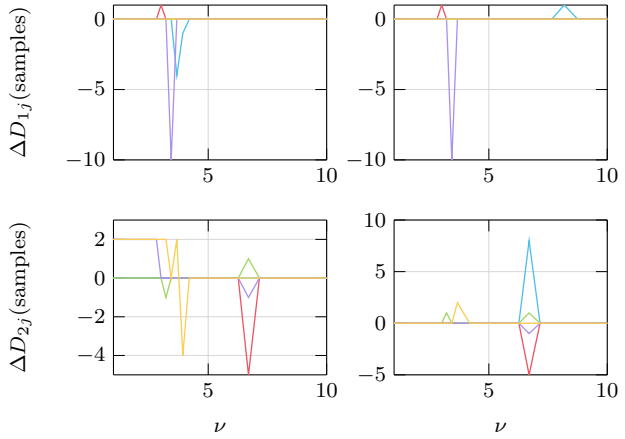

Fig. 4. Delay mismatches for time constant difference simulation of G_{11}.

3.6 Descussion of Results

From the results in Figs. 2 to 7, it is evident that the different simulation scenarios produce different ranges of compatibility between the presence of time constant differences and the PMR. For all variations of simulations, the ability of the PMR to detect parametric MPM dete-

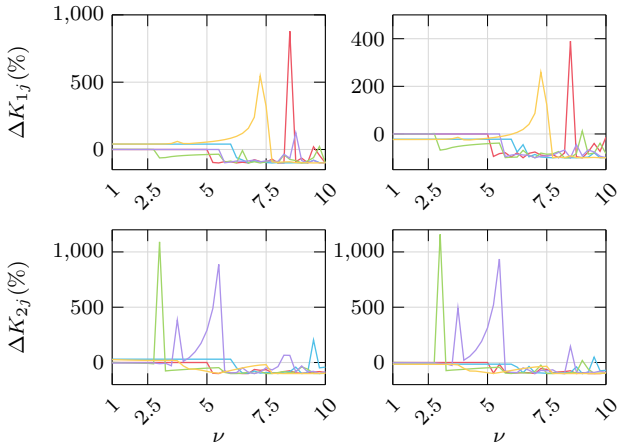

Fig. 5. Gain mismatches for time constant difference simulation of G_{12}.

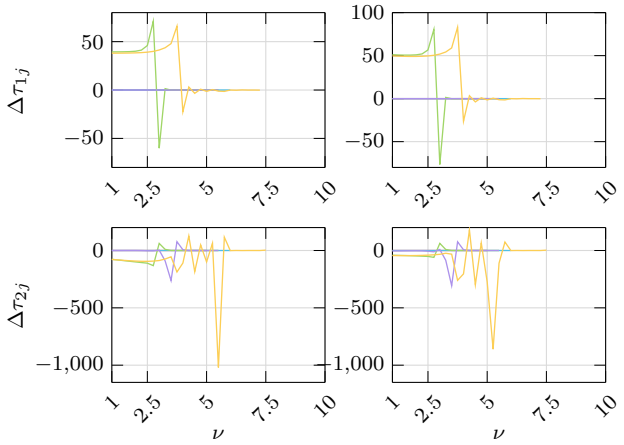

Fig. 6. Time constant mismatches for time constant difference simulation of G_{12}.

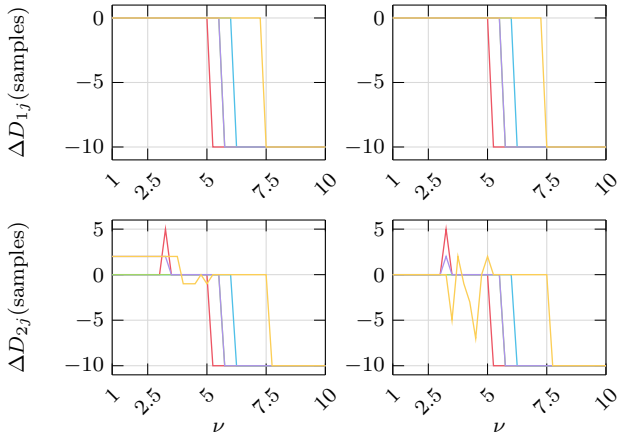

Fig. 7. Delay mismatches for time constant difference simulation of G_{12}.

riorates as ν increases. Therefore, it is observed that as the multivariable poles move away from one another, the PMR results become unstable.

It should be noted from the figures that the PMR starts to fail for G_{11} at about $\nu = 2.25$ and for G_{12} at about $\nu = 2.5$. For both of these multiplication factors the time constant differences between the transfer function being altered and the other transfer function in the same row is close to 1.8. Thus, for the Wood-Berry distillation column, the time constant differences between adjacent transfer functions should not exceed a factor of 1.8.

4. CONCLUSION

The SISO PMR, along with the improved PMR using an optimal delay estimation, as well as the expansion of the PMR to MIMO cases, was developed to help identify, isolate and diagnose parametric MPM for systems controlled by a model-based controller. The systematic diagnostic procedure, as captured in Table 1, along with the implicit method of estimating the PMR for MIMO cases, simplifies the PMR methodology as compared to the initial formulation of the PMR (Selvanathan and Tangirala, 2010; Yerramilli and Tangirala, 2016).

The PMR analysis was successfully validated as a viable method of diagnosing MPM on a 2×2 MIMO system using the Wood-Berry distillation column as seen in Section 3.3. Furthermore, the effects of time constant differences are investigated by using a multiplication factor applied to two separate time constants while the Wood-Berry distillation column is subject to various MPM scenarios. From the results of the simulations, the effects of time constant differences on the PMRs ability to accurately diagnose MPM are noted. For the specific case of the Wood-Berry distillation column the time constant differences, with a factor of 1.8 between transfer function time constants in the same row caused the performance of the PMR to deteriorate. Nonetheless, more systems would have to be investigated to quantitatively develop a general guideline for the application of the PMR to MIMO systems.

REFERENCES

Badwe, A.S., Gudi, R.D., Patwardhan, R.S., Shah, S.L., and Patwardhan, S.C. (2009). Detection of model-plant mismatch in MPC applications. *J. Process Contr.*, 19(8), 1305–1313.

Hamon, BV. and Hannan, EJ. (1974). Spectral estimation of time delay for dispersive and non-dispersive systems. *JRSS-C.*, 23(2), 134–142.

Jiang, H., Huang, B., and Shah, S.L. (2009). Closed-loop model validation based on the two-model divergence method. *J. Process Contr.*, 19(4), 644–655.

Kaw, S., Tangirala, A.K., and Karimi, A. (2014). Improved methodology and set-point design for diagnosis of model-plant mismatch in control loops using plant-model ratio. *J. Process Contr.*, 24(11), 1720–1732.

Li, L., Lu, L., Huang, Z., Chen, X., and Yang, S. (2020). A model mismatch assessment method of MPC by decussation. *ISA T.*, 106, 51–60.

Lindemann, M., Raethjen, J., Timmer, J., Deuschl, G., and Pfister, G. (2001). Delay estimation for cortico-peripheral relations. *J. Process Contr.*, 111(2), 127–139.

Ling, D., Zheng, Y., Zhang, H., Yang, W., and Tao, B. (2017). Detection of model-plant mismatch in closed-loop control system. *J. Process Contr.*, 57, 66–79.

Ljung, L. (1999). *System Identification: Theory for the User*. Prentice Hall Information and System Sciences Series. Prentice Hall PTR, Upper Saddle River, NJ, 2nd edition.

Mayne, D.Q. (2014). Model predictive control: Recent developments and future promise. *Automatica*, 50(12), 2967–2986.

Mittermaier, H.K. (2023). *Model-Plant Mismatch Diagnosis Using Plant Model Ratios for a Grinding Mill Circuit Under Model Predictive Control*. MEng Dissertation, University of Pretoria.

Mittermaier, H.K., Le Roux, J.D., Olivier, L.E., and Craig, I.K. (2023). Model-plant mismatch detection for a plant under Model Predictive Control: A grinding mill circuit case study. *IFAC-PapersOnLine*, 56(2), 11778–11783.

Oppenheim, A.V. (1999). *Discrete-Time Signal Processing*. Pearson Education, India.

Priestley, M.B. (1981). *Spectral Analysis and Time Series*. Academic Press, London; New York.

Qin, S. and Badgwell, T.A. (2003). A survey of industrial model predictive control technology. *Control Eng. Pract.*, 11(7), 733–764.

Schwenzer, M., Ay, M., Bergs, T., and Abel, D. (2021). Review on model predictive control: An engineering perspective. *Int. J. Adv. Manuf. Technol.*, 117(5), 1327–1349.

Selvanathan, S. and Tangirala, A.K. (2010). Diagnosis of poor control loop performance due to model-plant mismatch. *Ind. Eng. Chem. Res.*, 49(9), 4210–4229.

Skogestad, S. and Postlethwaite, I. (2010). *Multivariable Feedback Control: Analysis and Design*. Wiley, Chichester, 2nd edition.

Tsai, Y., Gopaluni, R.B., Marshman, D., and Chmelyk, T. (2015). A novel algorithm for model-plant mismatch detection for model predictive controllers. *IFAC-PapersOnLine*, 48(8), 746–752.

Wood, R.K. and Berry, M.W. (1973). Terminal composition control of a binary distillation column. *Chem. Eng. Sci.*, 28(9), 1707–1717.

Wu, Q. and Du, W. (2022). Online detection of model-plant mismatch in closed-loop systems with Gaussian processes. *IEEE T. Ind. Inform.*, 18(4), 2213–2222.

Xu, X., Simkoff, J.M., Baldea, M., Chiang, L.H., Castillo, I., Bindlish, R., and Ashcraft, B. (2020). Data-driven plant-model mismatch estimation for dynamic matrix control systems. *Int. J. Robust Nonlin.*, 30(17), 7103–7129.

Yerramilli, S. and Tangirala, A.K. (2016). Detection and diagnosis of model-plant mismatch in MIMO systems using plant-model ratio. *IFAC-PapersOnLine*, 49(1), 266–271.

Yerramilli, S. and Tangirala, A.K. (2018). Detection and diagnosis of model-plant mismatch in multivariable model-based control schemes. *J. Process Contr.*, 66, 84–97.

Yin, F., Wang, H., Xie, L., Wu, P., and Song, Z. (2014). Data driven model mismatch detection based on statistical band of Markov parameters. *Comput. Electr. Eng.*, 40(7), 2178–2192.